Electronic Supplementary Material (ESI) for RSC Advances.

Electronic supplementary information:

Multifunctional microparticles with uniform magnetic coatings and tunable surface chemistry

Tobias P. Niebel,[1] Florian J. Heiligtag,[2] Jessica Kind,[3] Michele Zanini,[1] Alessandro Lauria,[2] Markus Niederberger,[2] André R. Studart[1]

[1] Complex Materials, Department of Materials, ETH Zürich, 8093 Zürich, Switzerland

[2] Laboratory for Multifunctional Materials, Department of Materials, ETH Zürich, 8093 Zürich, Switzerland

[3] Laboratory of Metal Physics and Technology, Department of Materials, ETH Zürich, 8093 Zürich, Switzerland

Synthesis of nitrodopamine(ND) and nitrodopamine palmitate(ND-PA)

Materials and reagents: The following reagent-grade chemicals were purchased and used as received unless otherwise stated: N-hydroxy succinimide (NHS, 98%) and palmitoylchloride (PA-Cl, 98%) from ABCR (Germany), sodium nitrite ($NaNO_2$, min. 98% rectapur) from VWR (Switzerland), magnesium sulphate ($MgSO_4$, dried) from Fisher Chemicals (UK), tetrahydrofuran (THF, 99.5% extra dry over mole sieves) from Acros Organics (Belgium), 3-hydroxytyramine hydrochloride (dopamine), sulphuric acid (H_2SO_4, 95-97%), dichloromethane (DCM), ethylacetate (EtOAc) and ethanol (EtOH) from Sigma-Aldrich (Switzerland). Triethylamine (NEt_3, Acros, Belgium) was dried over molecular sieves. N,N-dimethylformamide (DMF, Merck, Germany) was dried by passing over columns of activated alumina using a solvent purification system (LC Technology Solutions Inc., Seabrook, USA). Deuterated dimethyl sulfoxide (DMSO-d_6, 99.8 atom % D, Eurisotop, France) and chloroform-d ($CDCl_3$, 99.8 atom % D, stabilized with Ag, Armar Chemicals, Switzerland) were used as received.

Nitrodopamine (ND) was synthesized according to the literature procedure:[1, 2] 5.07 g dopamine hydrochloride (26.7 mmol, 1 eq) and 4.03 g $NaNO_2$ (58.4 mmol, 2.2 eq) were dissolved in 66 ml deionized water and cooled with an ice/water bath. 2.5 ml H_2SO_4 (46.6 mmol, 1.7 eq) in 22 ml deionized water were added dropwise. The colour changed from orange to brown and a yellow solid precipitated. The reaction mixture was stirred overnight and allowed to warm to room temperature. The solid was collected by filtration over a G3

glass frit, washed with diluted H_2SO_4 and recrystallized from water. The product was collected as brown crystals of nitrodopamine hemisulfate and dried in an evacuated desiccator over silica gel (ND·$^1/_2$ H_2SO_4, 4.29 g, 17.4 mmol, 65.8%). ^{1}H-NMR (DMSO-d_6, 500 MHz, ppm): 7.46 (s, 1H, -C*H*-), 6.59 (s, 1H, -C*H*-), 3.08 – 3.00 (m, 4H, -CH_2-CH_2-). Elemental Analysis in weight % (calculated for $C_{16}H_{22}N_4O_{12}S$): C 38.12 (38.78), H 4.69 (4.48), N 11.31 (11.33).

N-hydroxy succinimide palmitoyl ester (NHS-PA) was synthesized in nitrogen atmosphere using Schlenk techniques according to a published procedure: [3] 2.0g NHS (17.4 mmol, 1.1 eq) were dissolved in 150 ml dry THF and 2.4 ml NEt_3 (17.4 mmol, 1.1 eq) were added. The mixture was cooled with an ice/water bath and 4.8ml PA-Cl (15.8 mmol, 1 eq) was added dropwise. The mixture was stirred for 3 h at room temperature. During this time a white precipitate was formed that was filtered off and washed twice with THF. The combined THF solutions were evaporated to dryness and the residue was re-dissolved in DCM. The resulting DCM solution was washed with 0.1 M HCl and twice with deionized water, before drying over $MgSO_4$ and removal of the solvent *in vacuo*. The crude product was purified by recrystallization from hot EtOAc as colourless crystalline flakes (NHS-PA, 4.85g, 13.7 mmol, 86.8%). ^{1}H-NMR ($CDCl_3$, 500 MHz, ppm): 2.86 – 2.80 (m, 4H, -N-C(O)-CH_2-), 2.60 (t, J = 7.5 Hz, 2H, -C(O)-CH_2-CH_2-), 1.74 (p, J = 7.7 Hz, 2H, -C(O)-CH_2-CH_2-), 1.43 – 1.35 (m, 2H, -C(O)-CH_2-CH_2-CH_2-), 1.34 – 1.23 (m, 22H), 0.87 (t, J = 6.9 Hz, 3H, -*C*H_3). ^{13}C{^{1}H}-NMR ($CDCl_3$, 126 MHz, ppm): 169.32 (-*C*(O)-N-*C*(O)-), 168.83 (-O-*C*(O)-), 32.07 (-*C*H_2-CH_2-CH_3), 31.09 (-C(O)-*C*H_2-CH_2-), 29.83 (-*C*H_2-), 29.80 (-*C*H_2-), 29.77 (-*C*H_2-), 29.74 (-*C*H_2-), 29.70 (-*C*H_2-), 29.58 (-*C*H_2-), 29.50 (-*C*H_2-), 29.39 (-*C*H_2-), 29.24 (-*C*H_2-), 29.21 (-*C*H_2-), 28.94 (-*C*H_2-), 25.74(-N-C(O)-*C*H_2-), 24.72 (-C(O)-CH_2-*C*H_2-), 22.84 (-*C*H_2-CH_3), 14.27(-*C*H_3). Elemental Analysis in weight % (calculated for $C_{20}H_{35}NO_4$): C 68.89 (67.95), H 10.49 (9.98), N 3.43 (3.96).

Nitrodopamine palmitate (ND-PA) was synthesized in nitrogen atmosphere using Schlenk techniques, following a procedure adapted from the synthesis of ND-PEG described elsewhere in the literature: [4] Using a 100 ml two neck round bottom Schlenk flask, 0.58g ND·$^1/_2$ H_2SO_4 (2.35 mmol, 1.1 eq) were dissolved in 30 ml dry DMF. 0.6 ml NEt_3 (4.32 mmol, 2 eq) were added and the mixture was cooled with an ice/water bath. 0.75 g NHS-PA (2.12 mmol, 1 eq) dissolved in 20 ml dry DMF were added dropwise over 15 minutes. The reaction mixture was stirred overnight while warming to room temperature. 150 ml acidified water (HCl) was added and the solution was extracted three times with 100 ml EtOAc. The combined organic phases were washed with 150 ml brine and with 150 ml deionized water, dried over $MgSO_4$ and reduced to a volume of ~100 ml using a rotary evaporator. The product precipitated as yellow powder when cooling in a refrigerator overnight. The yellow powder was collected by filtration, washed with cold EtOAc and dried in an evacuated

desiccator over silica gel (ND-PA, 0.70 g, 1.61 mmol, 75.8%). ^{1}H-NMR (DMSO-d_6, 500 MHz, ppm): 7.85 (t, J = 5.8 Hz, 1H, N*H*), 7.47 (s, 1H, -C(OH)-C*H*-CNO_2-), 6.66 (s, 1H, -C-C*H*-C(OH)-), 3.24 (dt, J = 7.6, 6.1 Hz, 2H, -C*H*$_2$-NH-), 2.87 (t, J = 7 Hz, 2H, -C-C*H*$_2$-CH_2-NH-), 1.99 (t, J = 7.5 Hz, 2H, -C(O)-C*H*$_2$-CH_2-), 1.43 (p, J = 7.3 Hz, 2H, -C(O)-CH_2-C*H*$_2$-), 1.23 (s, 24H), 0.85 (t, J = 6.8 Hz, 3H, -C*H*$_3$). ^{13}C{^{1}H}-NMR (DMSO-d_6, 126 MHz, ppm): 172.05 (-*C*(O)-), 151.54 (-C-CH-*C*(OH)-C(OH)-), 143.96 (-C(NO_2)-CH-*C*OH-), 139.25 (-*C*(NO_2)-), 128.12 (-*C*-), 118.25 (-C-*C*H-C(OH)-), 112.07 (-C(NO_2)-*C*H-C(OH)-), 38.92 (-NH-*C*H_2-), 35.41 (-C(O)-*C*H_2-), 32.86 (-*C*H_2-CH_2-CH_3), 31.29 (-C-*C*H_2-CH_2-NH-), 29.06 (-*C*H_2-), 29.03 (-*C*H_2-), 29.01 (-*C*H_2-), 28.91(-*C*H_2-), 28.78 (-*C*H_2-), 28.71 (-*C*H_2-), 28.67 (-*C*H_2-), 25.23 (-C(O)-CH_2-*C*H_2-), 22.10 (-*C*H_2-CH_3), 13.96 (-*C*H_3). Elemental Analysis in weight % (calculated for $C_{24}H_{40}N_2O_5$): C 65.50 (66.03), H 9.27 (9.23), N 6.37 (6.42).

Raman analysis of Fe_3O_4@Al_2O_3 platelets

Fe_3O_4@Al_2O_3 platelets synthesized by the sol-gel method in an oil bath were examined by Raman spectroscopy to gain further insight into the composition of the iron oxide phase (Figure S1). The main peak at 668 cm^{-1} can be assigned to the symmetrical Fe-O stretch (A_{1g}) of magnetite and provides thus further evidence that this is the phase of the iron oxide particles that coat the surface of the platelets.[5-7]

The spectrum was recorded using an InVia Raman Microscope from Renishaw (UK) at room temperature in backscattering configuration. The sample was excited with a green Ar laser at 532 nm and a laser power of 1%.

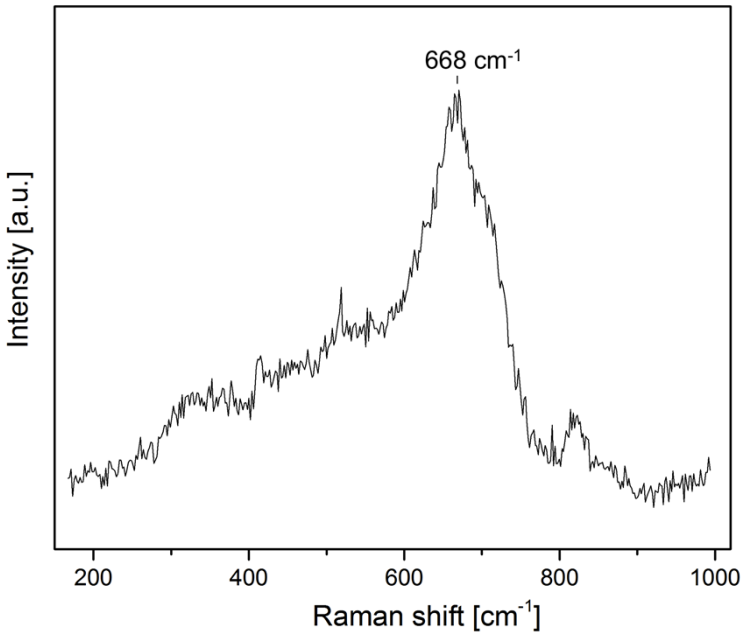

Figure S1: Raman spectrum of Fe_3O_4@Al_2O_3 platelets synthesized by the sol-gel method in an oil bath.

Absorption of nitrodopamine on microplatelets

The general procedure used to adsorb nitrodopamine on the surface of Al_2O_3 and Fe_3O_4@Al_2O_3 platelets is described in the experimental section of the main article. To quantify the amount of ND adsorbed on the platelets, the supernatant ND-solutions were measured with UV-Vis spectroscopy. Before the measurement the solutions were diluted to ensure that the detected absorbance values lie within the linear regime for which the Lambert-Beer law is valid.

To determine this linear range a series of samples with known ND concentrations in a background electrolyte of 0.01 mol/l KNO_3 and 0.01 mol/l HNO_3 was measured (Figure S2). The measured absorbance intensity associated with the HOMO→LUMO transition at 350 nm[8] is plotted against the known ND concentration of the solution (+ in Figure S3). Up to a ND content of 0.4 µmol/g there is a linear dependence of the measured absorbance at 350 nm on the concentration of ND in the supernatant solution. A non-linear dependence is observed for ND contents in the range 0.40 – 0.87 µmol/g. For concentrations higher than 0.87 µmol/g the instrument's detector saturates, leading to a cut off in the measured spectra. Note that µmol(ND)/g(solution) was chosen as unit for the ND concentration since the samples were weighed after every step to improve the accuracy of the analysis.

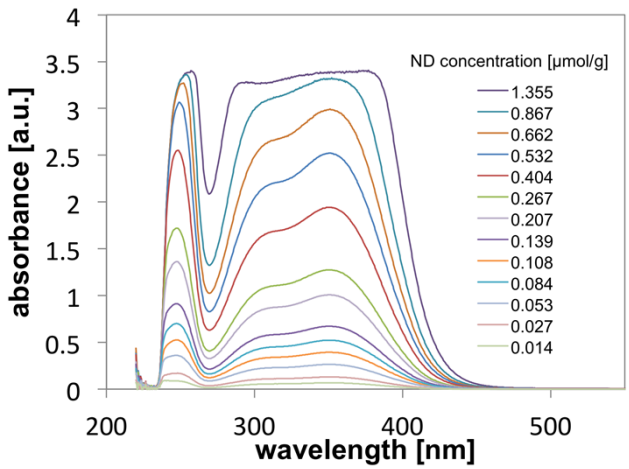

Figure S2: (a) UV-Vis spectra of solutions with different known ND concentrations and a fixed background electrolyte content of 0.01 mol/l KNO_3 and acid concentration of 0.01 mol/l HNO_3.

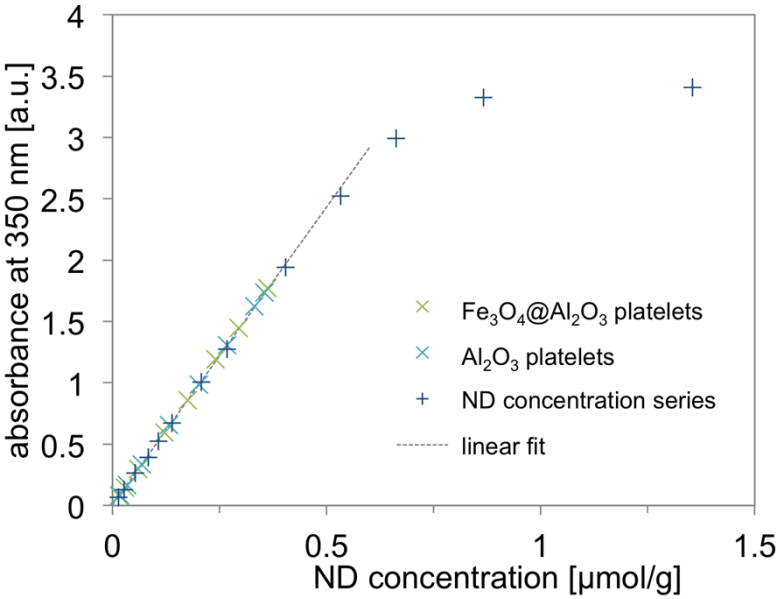

Figure S3: Absorbance intensity at the wavelength associated with the HOMO-LUMO transition for aqueous solutions with different known concentrations of ND. The adsorption solutions for Al_2O_3 and Fe_3O_4@Al_2O_3 platelets are in good agreement with the concentration series used to determine the linear absorbance regime.

The UV-spectra of the supernatant solutions before and after the adsorption of ND on Al_2O_3 and Fe_3O_4@Al_2O_3 platelets are shown in Figure S4. The solutions were diluted prior to the UV-Vis measurements to reduce the absorbance to levels below 2 (arbitrary units) and thus to ensure a linear correlation between the measured intensity and the ND concentration (Figure S3). After the measurement the spectra were multiplied with the dilution factor to account for small differences in the dilution and to enable quantitative analysis.

The adsorption densities of ND on the platelets were calculated from the ratios between the dilution-corrected absorbance maxima at 350 nm before and after the adsorption process, which are equivalent to the ratios between the ND concentrations in solution before and after their adsorption on the platelet surface (for details see Table S1).

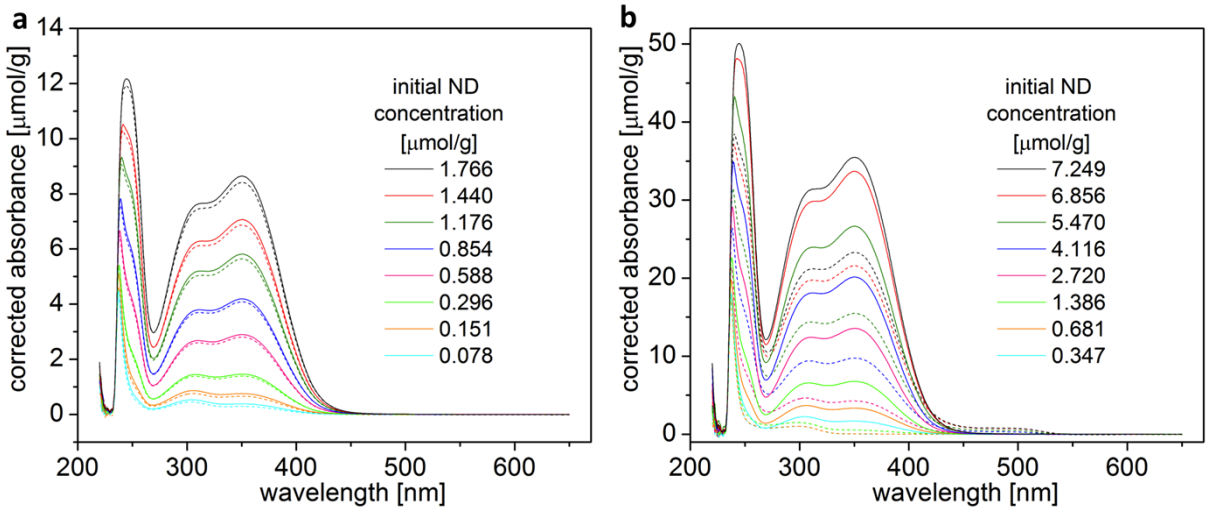

Figure S4: UV-Vis spectra of supernatant solutions before (full line) and after (dashed line) the adsorption of ND on (a) Al_2O_3 and (b) Fe_3O_4@Al_2O_3 at different initial ND concentrations. A fixed background electrolyte concentration of 0.01 mol/l KNO_3 and an acid concentration of 0.01 mol/l HNO_3 were used in all solutions. The spectra are multiplied with the dilution factor to allow quantitative analysis.

Table S1: Details and results for the calculation of ND adsorption densities on Al_2O_3 and $Fe_3O_4@Al_2O_3$ platelets.

initial conditions			before adsorption			after adsorption			calculation			results		
initial ND-concentration before adsorption [µmol/g]	used ND solution [g]	surface area of used platelets [m^2]	dilution factor	measured absorbance	dilution corrected absorbance	dilution factor	measured absorbance	dilution corrected absorbance	ratio of corrected absorbances	ND-concentration after adsorption [µmol/g]	amount of ND-adsorbed [µmol]	adsorption density [µmol/m^2]	equilibrium concentration of ND after adsorption [mmol/l]	
0.078	0.9735	0.144	4.93	0.0780	0.3847	4.85	0.0610	0.2958	0.7689	0.058	0.017	0.121	0.060	Al_2O_3 platelets
0.151	0.973	0.145	5.20	0.1456	0.7568	4.86	0.1363	0.6616	0.8742	0.128	0.018	0.127	0.132	
0.296	0.9743	0.145	4.90	0.2985	1.4625	4.87	0.2859	1.3932	0.9526	0.275	0.014	0.095	0.282	
0.588	0.9743	0.144	4.87	0.5949	2.8963	4.87	0.5766	2.8062	0.9689	0.555	0.018	0.124	0.570	
0.854	0.9745	0.143	4.88	0.8592	4.1921	4.79	0.8538	4.0857	0.9746	0.811	0.021	0.147	0.833	
1.176	0.9745	0.145	4.88	1.1909	5.8140	4.83	1.1692	5.6415	0.9703	1.112	0.034	0.235	1.141	
1.440	0.974	0.144	4.89	1.4456	7.0701	4.86	1.4132	6.8719	0.9720	1.363	0.039	0.274	1.400	
1.766	0.9742	0.143	4.87	1.7740	8.6448	4.84	1.7380	8.4126	0.9731	1.674	0.046	0.322	1.718	
0.347	0.9748	0.670	20.13	0.0837	1.6839	20.79	0.0027	0.0567	0.0337	0.011	0.327	0.488	0.012	$Fe_3O_4@Al_2O_3$ platelets
0.681	0.9752	0.675	20.30	0.1649	3.3482	20.09	0.0038	0.0761	0.0227	0.015	0.649	0.961	0.015	
1.386	0.9756	0.660	20.24	0.3348	6.7766	20.15	0.0276	0.5571	0.0822	0.111	1.241	1.879	0.114	
2.720	0.9682	0.670	20.65	0.6570	13.5675	20.09	0.2128	4.2758	0.3151	0.830	1.804	2.691	0.857	
4.116	0.9718	0.676	20.44	0.9857	20.1448	20.23	0.4829	9.7659	0.4848	1.939	2.061	3.048	1.995	
5.470	0.9702	0.668	20.41	1.3057	26.6543	20.09	0.7711	15.4952	0.5813	3.085	2.222	3.327	3.180	
6.856	0.9678	0.674	20.74	1.6249	33.6942	20.09	1.0746	21.5903	0.6408	4.251	2.383	3.538	4.393	
7.249	0.9691	0.674	20.46	1.7345	35.4834	19.81	1.1768	23.3160	0.6571	4.616	2.409	3.576	4.763	

Iron oxide coverage on Fe_3O_4@Al_2O_3 platelets

The magnetic susceptibility of Fe_3O_4@Al_2O_3 platelets coated with different amounts of iron oxide was measured as described in the main article. The amount of iron oxide on the surface of such platelets was tuned by changing the concentration of initial Fe precursors in the sol-gel solution or by varying the concentration of pre-formed iron oxide nanoparticles in the ferrofluid. To determine the actual coverage of Fe_3O_4 on the surface of the alumina platelets after the two coating processes (sol-gel and ferrofluid routes), we measured the mass fraction of Fe in Fe_3O_4@Al_2O_3 platelets by plasma-enhanced elemental analysis, as described in the main text. The obtained magnetic susceptibilities are plotted against the measured weight fraction of iron relative to the mass of iron oxide coated platelets in Figure S5.

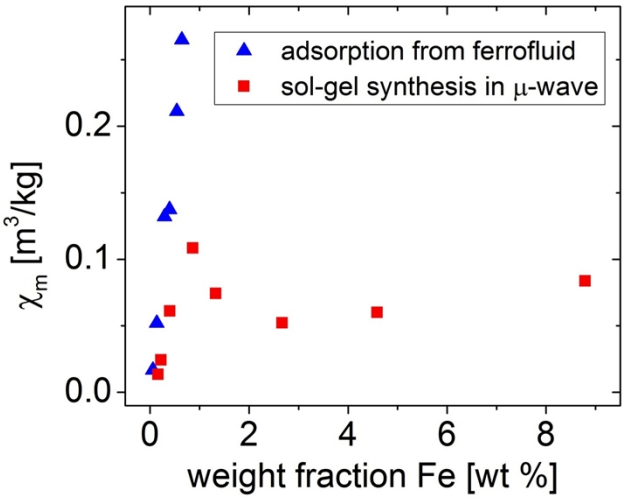

Figure S5: Magnetic susceptibilities for Fe_3O_4@Al_2O_3 platelets with varying amounts of iron oxide on the microparticle surface. Data from samples obtained using the sol-gel synthesis in a microwave are compared to those of specimens made through the adsorption of ferrofluid particles.

Since the magnetic susceptibility of such composite platelets is governed by the volume fractions of the magnetic material, we converted the measured weight fraction of Fe, $\omega(Fe)$, to the volume fraction of Fe_3O_4, $\phi(Fe_3O_4)$, using the following equation:

$$\phi(Fe_3O_4) = \frac{1}{1+\frac{\rho(Fe_3O_4)}{\rho(Al_2O_3)}\left(\frac{3M(Fe)}{\omega(Fe)\times M(Fe_3O_4)}-1\right)},$$

where $\phi(Fe_3O_4)$ is the volume fraction of Fe_3O_4 in the Fe_3O_4@Al_2O_3 platelets, $\omega(Fe)$ is the weight fraction of Fe in Fe_3O_4@Al_2O_3 platelets (measured value), $\rho(Fe_3O_4)$ is the density of magnetite (5.18 g/ml), $\rho(Al_2O_3)$ is the density of alumina (3.98 g/ml), $M(Fe)$ is the molar mass of iron (55.85 g/mol) and $M(Fe_3O_4)$ is the molar mass of magnetite (231.78 g/mol).

In these calculations, we assume that there are no other materials present in the composite platelets in addition to Fe_3O_4 and Al_2O_3. This approximation neglects the presence of surfactants on the ferrofluid nanoparticles and the possible partial oxidation of some of the iron oxide particles. The measured and calculated values for the iron and iron oxide concentrations as well as the measured susceptibilities are given in Table S2.

Table S2: Measured weight fraction $\omega(Fe)$, calculated volume fraction $\phi(Fe_3O_4)$ and measured magnetic susceptibility χ_m for Fe_3O_4@Al_2O_3 platelets with different iron oxide concentrations prepared by the sol-gel method or by adsorption of ferrofluid particles.

Weight fraction $\omega(Fe)$ [wt%]	Volume fraction $\phi(Fe_3O_4)$ [vol%]	Magnetic susceptibility χ_m [m^3/kg]	
8.79	9.61	0.084	sol-gel method
4.59	4.95	0.060	
2.67	2.86	0.052	
1.33	1.42	0.074	
0.86	0.92	0.108	
0.40	0.43	0.061	
0.22	0.23	0.024	
0.16	0.17	0.013	
0.64	0.68	0.265	ferrofluid
0.54	0.58	0.211	
0.40	0.42	0.137	
0.29	0.31	0.132	
0.14	0.15	0.052	
0.06	0.06	0.017	

As we have discussed in the main text, the ferrofluid approach cannot achieve an iron oxide concentration higher than 0.68 % vol. The SEM image of an alumina platelet with this maximum SPION concentration (Figure S6a) shows that this amount of iron oxide particles is not enough to lead to the dense and homogeneous layer of nanoparticles that we can achieve by our sol-gel approach (Figure S6b).

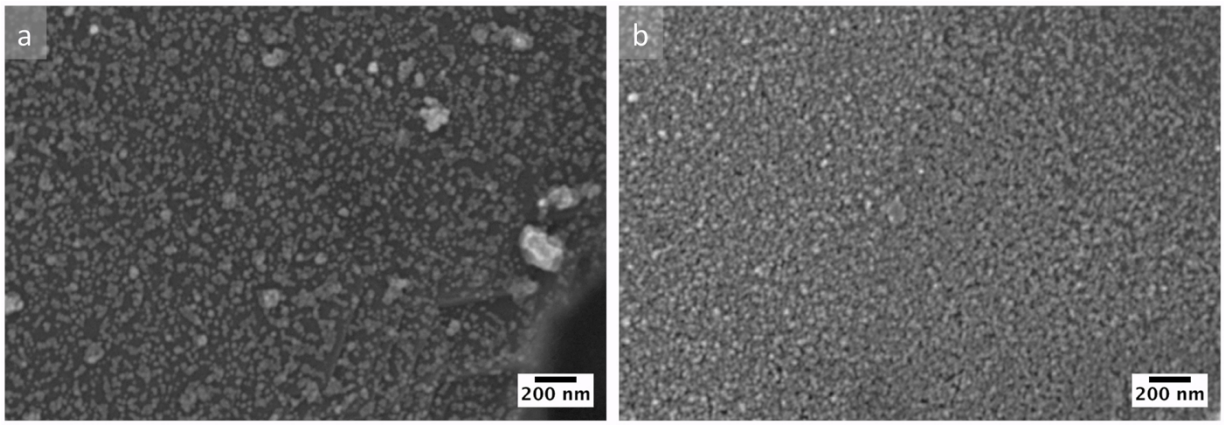

Figure S6: SEM images of an alumina platelets coated with iron oxide nanoparticles (a) at the maximum surface coverage achievable with the ferrofluid approach ($\phi(Fe_3O_4)$=0.68 % vol) as compared with (b) the complete and dense coating obtained with the sol-gel approach ($\phi(Fe_3O_4)$=2.86 % vol).

Wettability of modified platelets in different solvents

As a simple experiment to test the efficiency of the ND-PA coating of Fe_3O_4@Al_2O_3 platelets, different types of platelets were suspended in water or in chloroform (Figure S7). As-received Al_2O_3 platelets can be suspended both in water and in chloroform. However, after agitation of the suspensions, such bare platelets sediment much faster in the organic solvent than in water, which indicates a more hydrophilic character of the microparticle surface. The as-synthesized Fe_3O_4@Al_2O_3 platelets can be suspended in both solvents as well. In this case, faster sedimentation is observed in water rather than in chloroform. The lower hydrophilicity of Fe_3O_4@Al_2O_3 platelets probably results from the presence of some remaining benzyl alcohol groups on the platelet surface. By contrast, Fe_3O_4@Al_2O_3 platelets coated with ND-PA are not wetted by water and thus are only suspendable in chloroform. Even after extensive agitation in water the ND-PA modified platelets remain as a film on the water surface. This behaviour clearly shows that the ND-PA coating of Fe_3O_4@Al_2O_3 platelets was successful and renders the platelets hydrophobic.

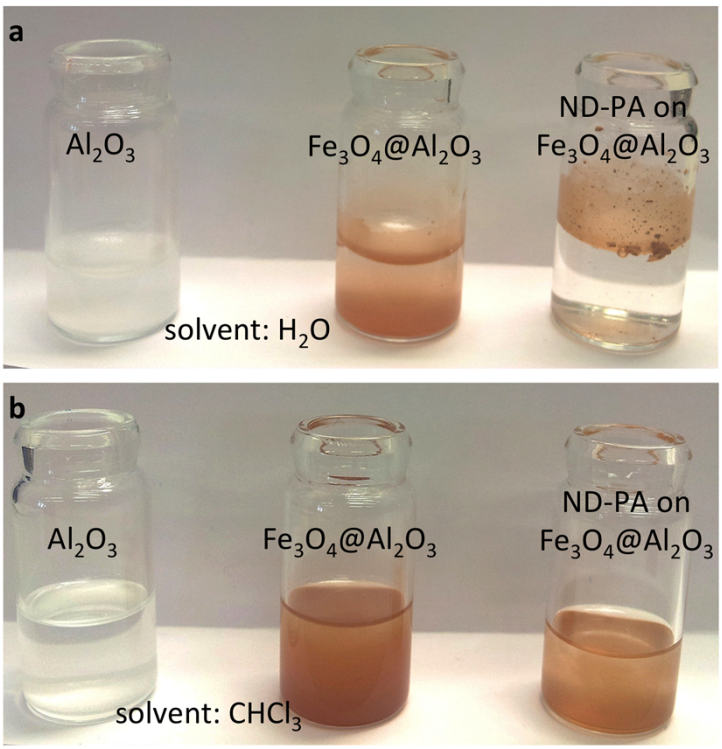

Figure S7: Al_2O_3 platelets, $Fe_3O_4@Al_2O_3$ platelets and ND-PA coated $Fe_3O_4@Al_2O_3$ platelets mixed with (a) water and (b) chloroform.

Scanning electron microscopy of as-received microparticles

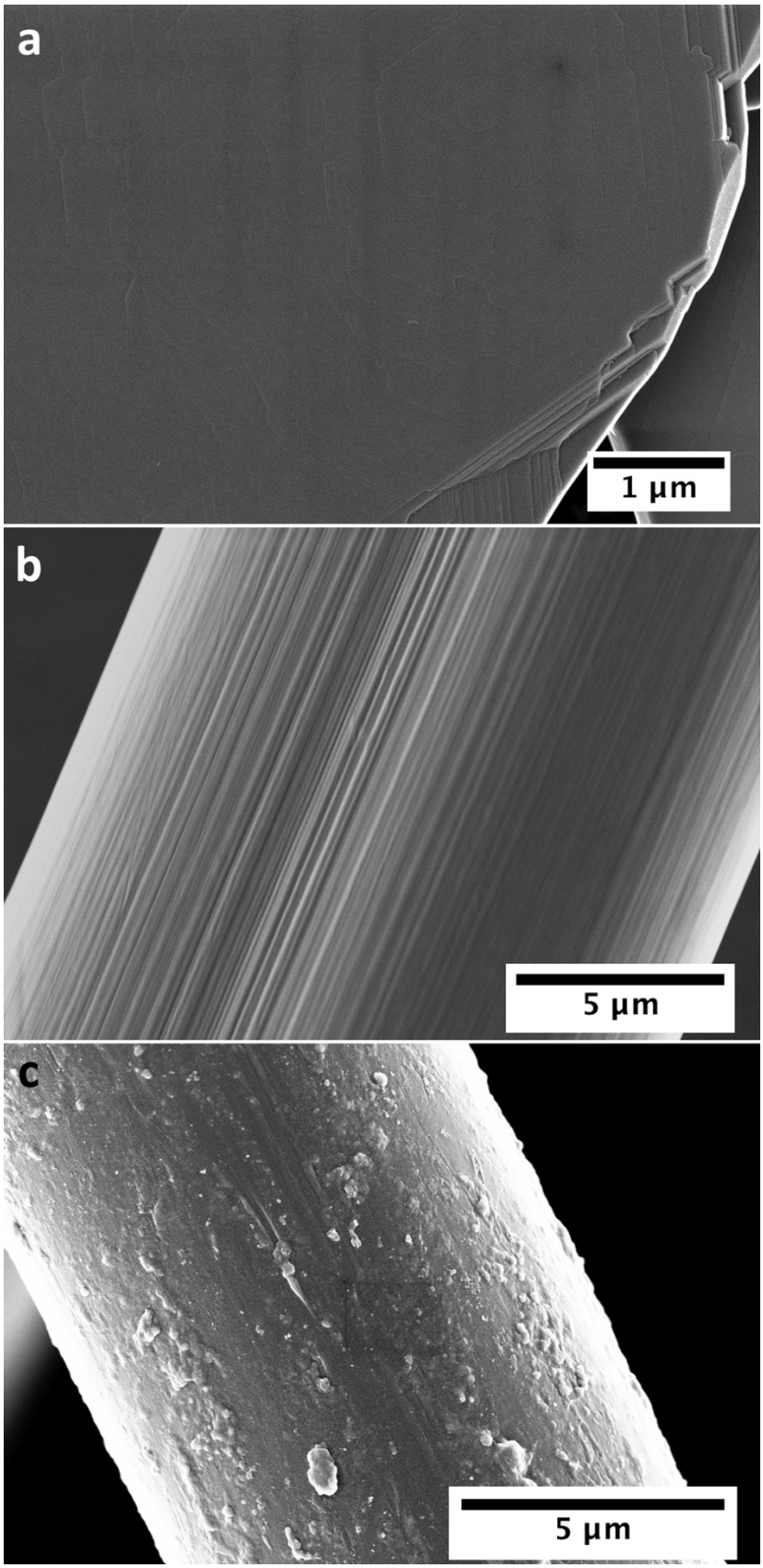

Figure S8: Scanning electron micrographs showing the uncoated surfaces of as-received (a) Al_2O_3 platelets (b) PVA fibres and (c) Aramid fibres.

References

1. A. Napolitano, M. d'Ischia, C. Costantini and G. Prota, *Tetrahedron*, 1992, **48**, 8515-8522.
2. B. Malisova, S. Tosatti, M. Textor, K. Gademann and S. Zürcher, *Langmuir*, 2010, **26**, 4018-4026.
3. J. Langecker, H. Ritter, A. Fichini, P. Rupper, M. Faller and B. Hanselmann, *ACS Appl. Mater. Interfaces*, 2012, **4**, 619-627.
4. T. Gillich, C. Acikgöz, L. Isa, A. D. Schlüter, N. D. Spencer and M. Textor, *ACS Nano*, 2012, **7**, 316-329.
5. N. Pinna, S. Grancharov, P. Beato, P. Bonville, M. Antonietti and M. Niederberger, *Chem. Mater.*, 2005, **17**, 3044-3049.
6. M. A. Legodi and D. de Waal, *Dyes and Pigments*, 2007, **74**, 161-168.
7. O. N. Shebanova and P. Lazor, *J. Solid State Chem.*, 2003, **174**, 424-430.
8. E. Amstad, A. U. Gehring, H. Fischer, V. V. Nagaiyanallur, G. Hähner, M. Textor and E. Reimhult, *J. Phys. Chem. C*, 2011, **115**, 683-691.